Emergent Materials (2023) 6:635–643
https://doi.org/10.1007/s42247-023-00463-6

ORIGINAL ARTICLE

Molybdate intercalated magnesium aluminium hydrotalcite as a potential catalyst for the oxidation of cinnamyl alcohol

M. Dipti Ranjan[1] · A. Sreenavya[1] · P. P. Neethu[1] · N. J. Venkatesha[2] · A. Sakthivel[1]

Received: 12 October 2022 / Accepted: 12 January 2023 / Published online: 1 February 2023

Abstract

Molybdate-intercalated magnesium aluminum hydrotalcite (Mg–Al–Mo HT) was prepared by a simple co-precipitation method. The synthesized materials were characterized by various analytical and spectroscopic techniques such as powder XRD, FT-IR, DRUV-visible, TGA, NH_3-TPD, FE-SEM, and nitrogen sorption studies. The catalytic activity of Mg–Al–Mo HT material was explored for the oxidation of lignin-derived cinnamyl alcohol. The reaction was carried out in the presence of tertiary butyl hydrogen peroxide (TBHP) in decane as an oxidant under ambient conditions (110 °C and 6 h). The catalyst showed excellent activity with 70% conversion of cinnamyl alcohol with the formation of epoxy cinnamyl alcohol as the major product. The catalyst retains its activity even after the fourth cycle. The Mg–Al–Mo HT was found to be a superior catalyst for the oxidative conversion of lignin model compounds to value-added chemicals.

Keywords Molybdate · Epoxy cinnamyl alcohol · Lignin · Hydrotalcite · Oxidation

1 Introduction

Hydrotalcites (HT) are materials derived from edge-shared double hydroxide layered materials with divalent and trivalent metal ions in the framework sites having interlayer anions [1–10]. HT materials having flexible framework cations facilitate tuning their surface acid–base and redox properties and are known to be potential support for the uniform deposition of the nanoparticles [1–13]. HT materials in their as-prepared and calcination forms (solid solution of mixed metal oxide) have intrinsic surface basicity and redox properties, which have been extensively utilized for various catalytic processes [1–13]. In this regard, it is important to note that early transition metals such as V, Mo, and W are known as excellent candidates for various catalytic processes. However, it is challenging to incorporate these elements in the framework of HT due to the variation in ionic size and geometrical adaptation. On the other hand, the anionic forms such as vanadates, molybdates, and tungstates have been successfully intercalated to the interlayer of HT and explored for their potential functions [1–5]. HT derived from divalent magnesium and trivalent aluminum framework species (Mg–Al HT) is known as the potential material for base-catalyzed reactions, particularly isomerization of glucose to fructose [6], aldol condensations [7], the Knoevenagel reaction, CO_2 methanation [8], epoxidations [9], and trans-esterifications, etc. Mg–Al HT containing silicate, molybdate, vanadate, and phosphate [10–13] in the interlayer region enhances the number of active sites and improves the catalytic efficiency of the materials. Several Mo-containing HTs were proven to be active catalysts for different reactions such as selective olefin oxidation, oxidative dehydrogenation of propane [14], oxidation metathesis [15], C–H activation, epoxidation [16], dehydration, trans-esterification, tertiary butanethiol oxidation [17], and anti-corrosion reactions [18, 19], etc. Molybdate anions exist mainly as $[MoO_4]^{2-}$, $[Mo_7O_{24}]^{6-}$, and $[Mo_2O_7]^{2-}$ in the interlayer region based on the pH of the synthesis gel [20] and vary its catalytic properties.

Recently, the oxidation of cinnamyl alcohol (COL) using aerobic oxygen has received considerable attention

M. Dipti Ranjan, A. Sreenavya and P. P. Neethu contributed equally.

✉ A. Sakthivel
sakthivelcuk@cukerala.ac.in

[1] Inorganic Materials & Heterogeneous Catalysis Laboratory, Department of Chemistry, School of Physical Sciences, Sabarmati Building, Tejaswini Hills, Central University of Kerala, Kasaragod-671320, India

[2] Post Graduate Department of Chemistry, Visveswarapura College of Science, Bangalore Institute of Technology, K.R. Road, V.V.Pura, Bengaluru 560004, India

in producing bulk and specialty chemicals from renewable feedstocks. COL is a biomass model component with aromatic and allylic alcohol functionality and is found naturally in the inner bark of cinnamon trees. The oxidation of COL is used as a probe reaction to assess the selective activation of the OH group or the C–C double bond [21, 22]. Cinnamyl alcohol is a molecule containing multiple functionality, viz., reactive hydroxyl and alkene groups, leading to complex reaction mechanisms during the redox processes. The preferred oxidation product is a carbonyl compound, which is cinnamaldehyde (CAL) and has a wide range of applications such as cinnamon flavor in food and fragrance industries, insecticide, animal repellants, flea repellent, plant protection against nematodes, antibacterial agents, and agricultural chemicals such as fungicides and insecticides [23]. During the oxidation of COL using these oxidants, oxy-functionalized olefins (i.e., epoxy cinnamyl alcohol) are also formed as a byproduct, which is a useful intermediate in organic synthesis [22].

The catalytic activity of different heterogeneous catalysts explored for the oxidation of COL and their product distributions are summarized in Table S1. Noble metals (Pt, Pd, and Au) are active catalysts in the liquid phase oxidation of alcohols. Because of their high catalytic performance, noble metal catalysts were used to study most of the COL oxidation reactions, particularly Pd- and Au-based catalysts. However, considering the low natural abundance and the high cost of noble metals, developing non-precious metal catalysts for the aerobic oxidation of alcohols is needed for the sustainable chemical industry. The literature has reported that TBHP is a superior oxidant for the liquid phase oxidation of COL because of the higher reactivity compared with O_2 and the higher stability compared to H_2O_2 [30]. The oxidizing ability of TBHP depends strongly on the solvent used. Toluene, acetonitrile, and methanol are the most commonly used solvents for COL oxidation [24, 25, 31]. Recently, hydrotalcite (HT)-based catalysts for oxidation reactions have attracted attention because of their considerable catalytic activity and their vast potential to be used as substitutes for noble metal catalysts. Neethu et al. studied the oxidation of cinnamyl alcohol using ruthenium on α $Ni(OH)_2$ as the catalyst at 90 °C and reported 84% conversion of cinnamyl alcohol and 80% selectivity of cinnamaldehyde [28]. HT and their derivative compounds are useful for achieving alcohol oxidations under environmentally suitable conditions [32–34]. The molybdenum in its higher oxidation state presents as molybdate species having Mo = O moieties, which can be converted to peroxo-species in the presence of peroxide, known as the most active catalyst for oxidation of olefin, ammoxidation, etc. [32–36]. The oxophilic nature of molybdate species promotes strong interaction with peroxide and forms peroxo-species, which are extensively explored for the oxidation of various organic functionalities [32–36]. Therefore, in this work, we focused on developing molybdate ion-intercalated HT (Mg–Al–Mo HT) and explored its applications in the oxidation of cinnamyl alcohol to epoxy cinnamyl alcohol and cinnamaldehyde.

2 Experimental

2.1 Materials

Magnesium nitrate hexahydrate ($Mg(NO_3)_2.6H_2O$, 98%; LOBA), aluminum nitrate nonahydrate ($Al(NO_3)_2.9H_2O$, 98%; LOBA), ammonium heptamolybdate tetrahydrate ($(NH_4)_6Mo_7O_{24}.4H_2O$, 99%; Merck), ammonia solution (NH_4OH, 25%; SRL), cinnamyl alcohol (98%; LOBA), toluene (99%; SRL), isopropyl alcohol (99%; SRL), acetonitrile (99.5%; Merck), tertiary butyl alcohol (99.5%; Merck), hydrogen peroxide (30% solution in water), TBHP in water (70% in water, Merck), and TBHP in decane (5.5 M in decane, Aldrich).

2.2 Catalyst preparation

The Mg–Al–Mo HT catalyst was synthesized by the co-precipitation method followed by hydrothermal treatment. Solution-A was prepared by dissolving $Mg(NO_3)_2.6H_2O$ (45.45 mmol) and $Al(NO_3)_2.9H_2O$ (15 mmol) in 120 mL water. Solution-B was prepared by dissolving $(NH_4)_6Mo_7O_{24}.4H_2O$ (4.545 mmol) in 100 mL deionized water and 10 mL of ammonia solution. Furthermore, solution-B was added in a dropwise manner into solution-A with constant stirring at 65 °C for 2 h. The formation of a precipitate was observed with a final gel pH of 8.4, and the resulting solution was transferred into an autoclave for hydrothermal treatment at 100 °C for 4 days. The precipitation of Mg–Al–Mo HT gel was filtered and washed repeatedly with deionized water until the pH of the filtrate was 7. The material was dried overnight at 80 °C and represented as Mg–Al–Mo HT. Based on the molar concentration of molybdate anion, the as-prepared samples are labeled as Mg–Al–Mo HT0.1 and Mg–Al–Mo HT0.15, respectively, containing 0.1 and 0.15 mol of molybdate. Until specified, the sample used in the present study is Mg–Al–Mo HT0.1. The obtained Mg–Al–Mo HT was calcined at 400, 600, and 800 °C for 4 h. The catalyst prepared at different calcination temperatures is represented as Mg–Al–Mo HT400, Mg–Al–Mo HT600, and Mg–Al–Mo HT800. For comparison, the parent magnesium–aluminum hydrotalcite was also prepared and represented as Mg–Al HT.

2.3 Material characterization

FT-IR spectrum of synthesized catalyst is recorded on Jasco 4000 FT-IR spectrum by ATR technique. The spectra obtained 4 cm^{-1} resolution and 60 scans in the middle IR region, i.e.; (400–4000 cm^{-1}). Powder X-ray diffraction of catalyst is recorded using Rigaku-Miniflex 600 diffractometer using nickel-filtered CuKα radiation and a liquid-nitrogen-cooled germanium solid-state detector. The diffraction pattern was recorded in the 2θ range of 3 to 90° in step size of 0.02°. The size and morphology of the hydrotalcite materials were measured using Zeiss Gemini SEM 300 EDS detector EDX. The UV–visible spectrum of the catalyst is recorded with Shimadzu UV 2500 spectrometer. $BaSO_4$ compound is used as blank for solid samples, and TPD analysis was carried out by using BELCAT-M (Japan) instrument. This is used to determine the acidity properties of a solid catalyst. N_2 adsorption–desorption measurements were carried out using an automatic micropore physisorption analyzer (Micromeritics ASAP 2020, USA) after the samples were degassed at 250 °C for 10 h. Thermogravimetric analysis of the sample was carried out using Perkin-Elmer STA 6000 in air/oxygen with 2–5 mg of the sample and with a heating rate of 10 °C min^{-1} in the temperature range of 31–900 °C.

2.4 Oxidation reaction

The oxidation reaction of cinnamyl alcohol was carried out in a glass batch reactor (50 mL). For this process, 0.05 g of the catalyst was preheated for activation at 100 °C for 1 h. In a typical reaction, 2 mmol (0.25 mL) of cinnamyl alcohol, 0.05 g of the catalyst, and 1 mL of toluene as solvent was taken in a glass batch reactor. The reaction mixture was heated at the desired temperature with continuous stirring. When the reaction mixture attained the desired reaction temperature, 2 mmol of TBHP in decane was added, and the reaction was further continued for 6 h. When the reaction was completed, the liquid products were separated by filtration. The products were analyzed by gas chromatography (Mayura Analytical 1100 series) equipped with AB5 capillary column and flame ionization detector. The products were also confirmed by gas chromatography-mass spectrometry (GC–MS) and nuclear magnetic resonance (^{1}HNMR) analysis (Figs. S4, S5, and S6).

3 Results and discussion

3.1 Characterization of the catalyst

The FTIR spectrum of the sample analyzed in the range of 400–4000 cm^{-1} is presented in Fig. 1. Mg–Al–Mo HT showed a broad absorption band at 3316 cm^{-1}, which can be attributed to the stretching vibrations of the hydrogen-bonded hydroxyl group present in the brucite-like layer. The bending vibration of the interlayer water molecules occurs at 1631 cm^{-1}; both these vibrational bands support the presence of an excess of adsorbed water molecules present in the interlayer region. A broadband appeared at 920 cm^{-1} and is assigned to the vibrations of Mo = O in molybdate MoO_4^{2-}, which is present in the interlayer region. A small amount of carbonate (CO_3^{2-}) anion is also present in the interlayer region, which is evident from the peak observed around 1366 cm^{-1}. A band at 670 cm^{-1} with a shoulder at 856 cm^{-1} is typically characteristic of the Mo–O–Mo stretching vibration of MoO_4^{2-} in the interlayer region. The lower wavenumber band at 546 and 450 cm^{-1} is assigned to the lattice vibrations of Mg–O and Al–O bonds [19].

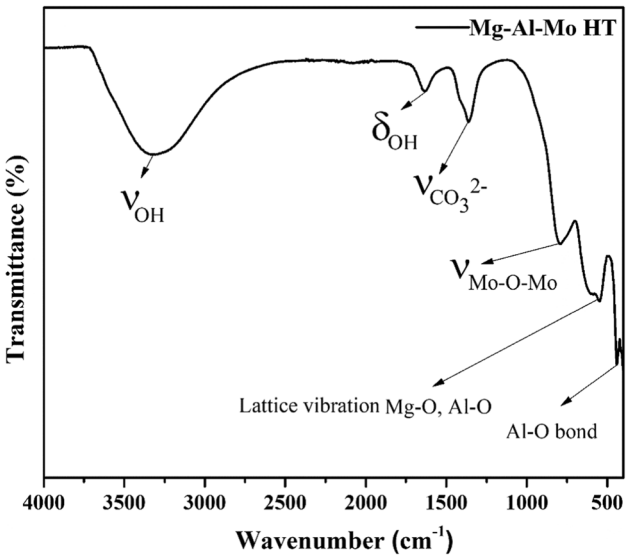

Fig. 1 FT-IR spectrum of Mg–Al–Mo HT

Powder X-ray diffraction patterns of Mg–Al HT and Mg–Al–Mo HT are displayed in Fig. 2. The samples exhibited main reflection planes, which are typical characteristics of HT materials. Two sharp and symmetric peaks at low 2θ of 11.20 and 22.49° are essentially assigned to the reflections by the basal planes of (003) and (006), respectively. The other broad and asymmetric peaks at 2θ of 34.25, 38.24, 45.53, 60.23, and 61.37° correspond to the reflections by the basal planes of (012), (015), (018), (110), and (113), respectively, confirming the formation of a crystallized layered HT structure. X-ray reflection signals of the Mg–Al–Mo HT sample are somewhat broader and noisier than that of the parent Mg–Al HT, as seen in Fig. 2. The "c" parameter of the Mo-containing HT is higher than that of the parent hydrotalcite Mg–Al HT, reflecting the successful intercalation of MoO_4^{2-} anions into the interlayer

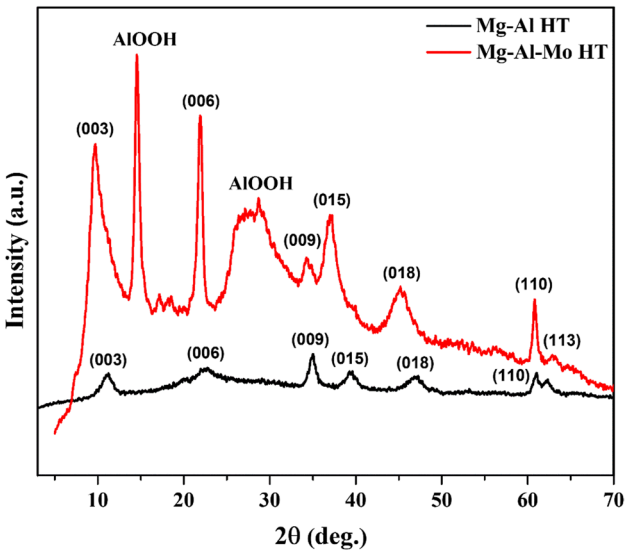

Fig. 2 Powder XRD patterns of Mg–Al HT and Mg–Al–Mo HT

spaces between (Mg, Al) brucite-like sheets [19, 37]. The UV–visible spectrum of Mg–Al–Mo HT (Fig. S1) displays an absorption band observed in the region of 248 nm, which can be described as the charge transfer of O^{2-} to Mo^{6+} of the isolated MoO_4^{2-} species with Mo in the tetrahedral coordination. The broad shoulder band observed near the edge of the band is characteristic of molybdenum polyoxoanions [38, 39].

The morphology of the Mg–Al–Mo 0.1A and Mg–Al–Mo 0.15A hydrotalcite materials is shown in the SEM images presented in Fig. 3. The SEM images of both samples are aggregates of smaller irregular shapes with rough surfaces in nature. The particles are an aggregation of platy sheets of crystallites in nature, which are characteristics of HT materials having layered structures. The surface composition of the material was determined by EDX (Figs. S2 and S3) analysis. Table S2 shows a uniform distribution of molybdate species on the surface of layered materials. The NH_3-TPD result of Mg–Al–Mo HT is shown in Fig. 4. The sample exhibited desorption peaks at 160 and 505 °C, indicating the presence

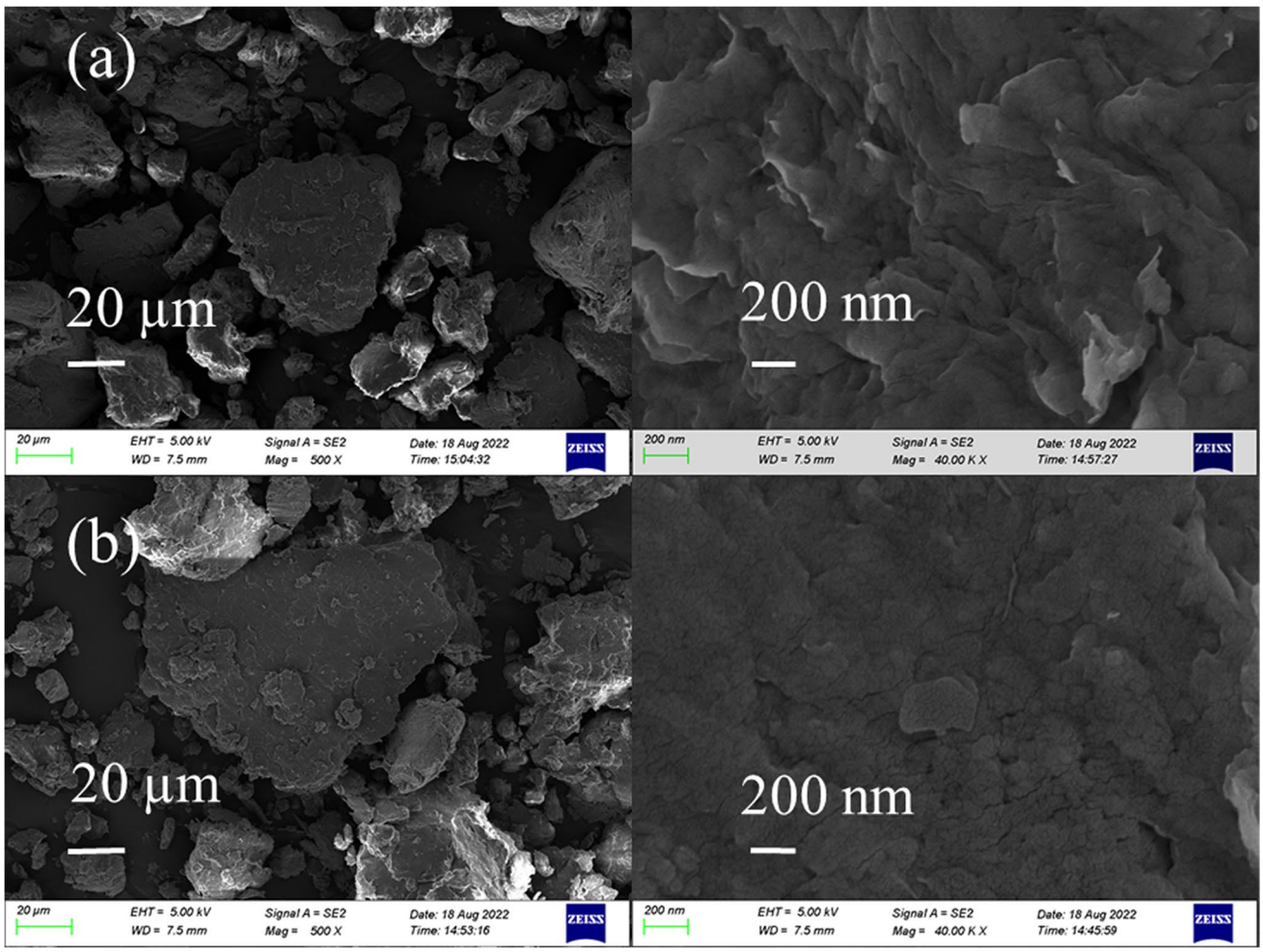

Fig. 3 FE-SEM images of **a** Mg–Al–Mo HT 0.1 and **b** Mg–Al–Mo HT 0.15

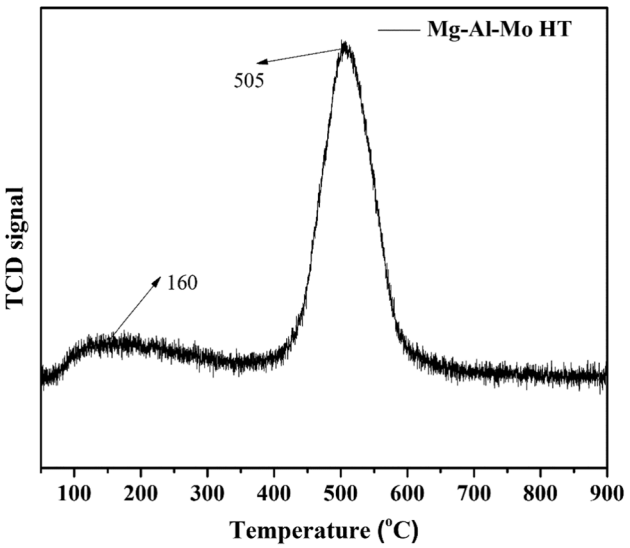

Fig. 4 TPD profile of Mg–Al–Mo HT

of weak and strong acidic sites, respectively. The area corresponding to the high-temperature desorption peak represents 0.012 mmol.g^{-1} acidic sites, which are present in the materials. The N_2 adsorption–desorption isotherm of Mg–Al HT and Mg–Al–Mo HT is shown in Fig. 5, and the textural properties of the materials are given in Table S3. The parent Mg–Al HT has the characteristics of the type-IV isotherm with H4 hysteresis, and the Mg–Al–Mo HT exhibited multilayer adsorption in the relative pressure (p/p_0) range of 0.1–1, which is characteristic of the type-IV isotherm with H3 hysteresis indicating the mesoporous nature of the material, which is evident from the pore size distribution [40].

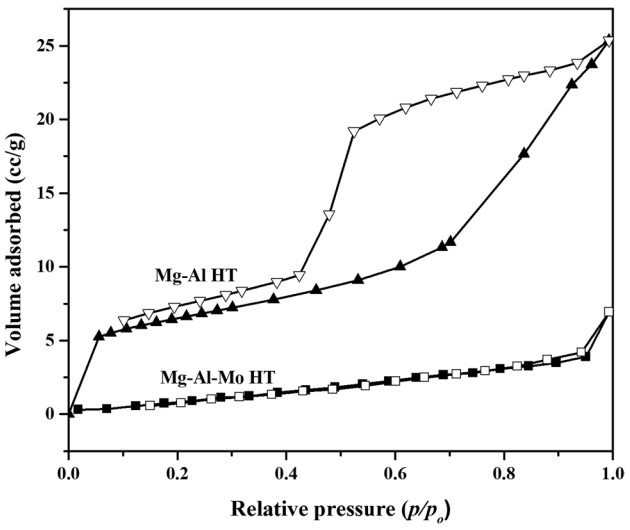

Fig. 5 N_2 adsorption–desorption profiles of Mg–Al and Mg–Al–Mo HT

The thermal behavior of the synthesized material was studied using thermogravimetric analysis (TGA). The TGA profile of the as-synthesized and used Mg–Al–Mo HT is displayed in Fig. 6. The as-synthesized Mg–Al–Mo HT catalyst exhibits a three-stage thermal decomposition. The first stage of weight loss of 6% occurs at a low temperature of approximately 80–160 °C due to the elimination of physisorbed water molecules present in the interlayer region of HT. The second stage weight loss (8%) observed in the temperature range between 160 and 260 °C is due to the removal of chemisorbed water from the internal and external surfaces of the structure. The third stage of weight loss occurs up to 500 °C and is attributed to the removal of hydroxyl groups from the brucite-like layer and the loss of interlayer carbonate anions in the form of CO_2. The used catalyst shows a rapid weight loss in the temperature range of 450 – 650 °C, which may be due to the removal of adsorbed organic species on the surface of the catalyst.

3.2 Cinnamyl alcohol oxidation over Mg–Al–Mo HT catalyst

The cinnamyl alcohol oxidation over the Mg–Al–Mo HT catalyst was studied with different oxidants such as H_2O_2 (30%), TBHP in water, and TBHP in decane at 90 °C for 6 h. The results are summarized in Fig. 7. The use of an organic oxidant in organic solvent, viz., TBHP in decane, showed better results. It is clear from the results that the reaction using tertiary-butyl hydroperoxide in decane shows better COL conversion (29%) with 71% selectivity of CAL and a minor quantity of epoxy cinnamyl alcohol. The products of COL oxidation were confirmed by GC–MS (Fig. S4) and ^{1}H-NMR analysis (Figs. S5 and S6). The ^{1}H-NMR spectrum of the isolated major products has signals

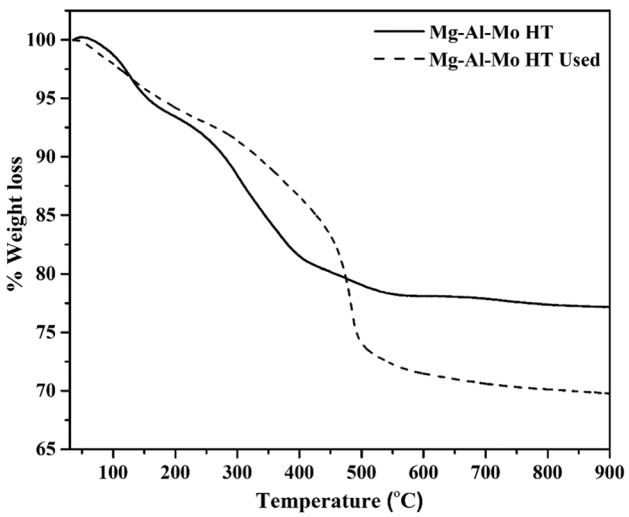

Fig. 6 TGA profiles of as-synthesized and used Mg–Al–Mo HT

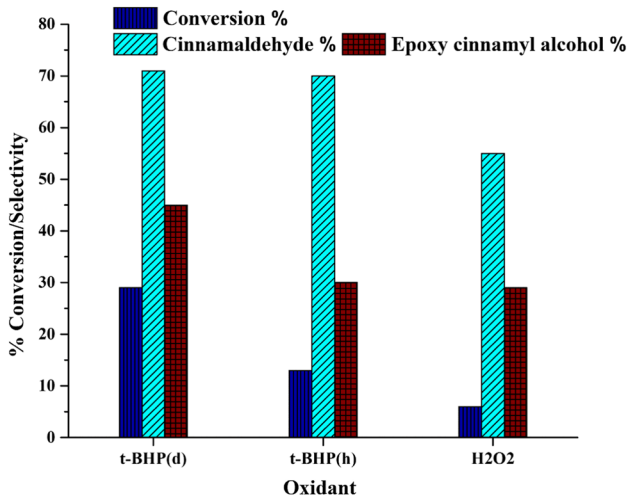

Fig. 7 Effect of different oxidants on cinnamyl alcohol oxidation over Mg–Al–Mo HT catalyst.[#] Reaction conditions: 2 mmol COL, 2 mmol oxidant, 0.05 g catalyst, 90 °C, and 6 h

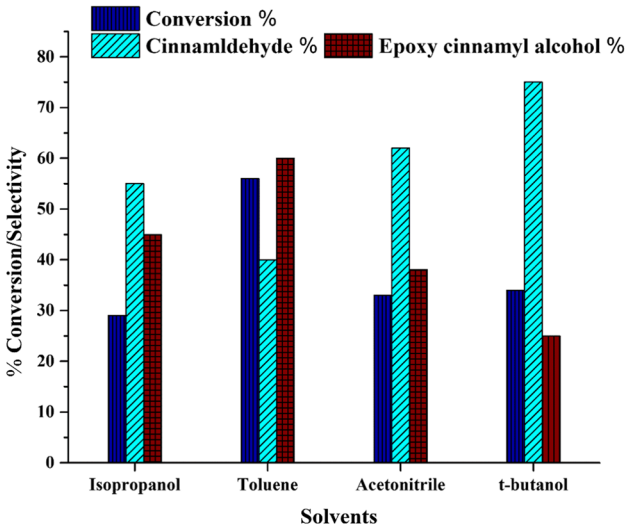

Fig. 8 Effect of solvents on cinnamyl alcohol oxidation over Mg–Al–Mo HT catalyst. [#]Reaction conditions: 2 mmol COL, 2 mmol oxidant, 1 mL solvent, 0.05 g catalyst, 90 °C, and 6 h

in aromatic, aliphatic, aldehyde, epoxide, and alcohol regions. The NMR spectrum shows nine proton peaks that match with the protons of cinnamaldehyde (δH (500 MHz), $CDCl_3$); 7.78 (3H, d, ArH), 7.46 (2H, d, ArH), 7.38 (1H, d, aliphatic H), 6.74 (1H, d, aliphatic H), and 9.73 (1H, d, aldehyde H)). The other major product, viz., epoxy cinnamyl alcohol, was also confirmed by ^{1}H-NMR (500 MHz, $CDCl_3$); 7.60–7.08 (5H, m, ArH), 3.81 (1H, s, epoxide H), 2.75 (1H, t, epoxide H), 4.29 (2H, t, CH), and 2.02 (1H, t, OH) [22].

The reaction using TBHP in water and aqueous hydrogen peroxide showed a low conversion, i.e., 6 and 13%, respectively. As the molybdate ion is oxophilic in nature, the presence of water masks the active sites of the catalyst, resulting in a decrease in the conversion and selectivity. Thus, for further studies on COL oxidation over the Mg–Al–Mo HT catalyst, TBHP in decane was chosen as an oxidant. The effect of solvents on the catalytic conversion of COL oxidation using Mg–Al–Mo HT was studied using various solvents. The results are displayed in Fig. 8. The reaction was carried out using various solvents such as isopropyl alcohol, toluene, acetonitrile, and tertiary-butyl alcohol, and 29, 56, 33, and 34% conversion, respectively, was obtained. Among the various solvents studied, the use of the nonpolar solvent, toluene gave the best result with 56% conversion of COL and 40 and 60% selectivity for CAL and epoxy cinnamyl alcohol, respectively. A nonpolar organic solvent facilitates better catalytic conversion. The use of polar solvent molecules may solvate the active species and reduces the conversion. The reaction in solvent-free conditions shows 29% conversion. From the solvent study, it is clear that the reaction obtained maximum conversion in the presence of a solvent. Chemical transformations occur at a solid–liquid interface where the adsorbate species are influenced by the interaction with the solvent. Thus, the reaction was carried out with toluene as a solvent for the further studies.

The COL oxidation using the Mg–Al–Mo HT catalyst was performed at varying reaction temperatures from 90 to 120 °C. The results are displayed in Fig. 9. The reaction exhibited improved conversion at every reaction temperature, and a maximum conversion of 74% at 110 °C with 70% selectivity for epoxy cinnamyl alcohol and 30% selectivity for CAL

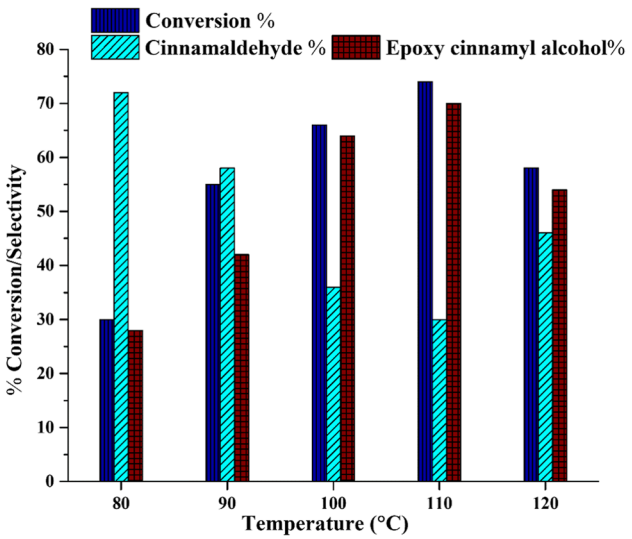

Fig. 9 Effect of reaction temperature on cinnamyl alcohol oxidation over Mg–Al–Mo HT catalyst using toluene as solvent. [#]Reaction conditions: 2 mmol COL, 2 mmol oxidant, 1 mL toluene, 0.05 g catalyst, and 6 h

was observed. A decrease in conversion was observed when the reaction temperature was further increased.

The COL reaction was further studied using the Mg–Al–Mo HT catalyst after calcining at various temperatures such as 400, 600, and 800 °C. The results are displayed in Fig. 10. Among the various catalysts, the Mg–Al–Mo HT800 catalyst shows better catalytic activity. Mg–Al–Mo HT800, Mg–Al–Mo HT600, and Mg–Al–Mo HT400 catalysts showed 83, 44, and 40% cinnamyl alcohol conversion, respectively, at 110 °C for 6 h. However, as the calcination temperature increases, a decrease in the selectivity of CAL is observed. Calcining the catalyst at 800 °C for 4 h results in the formation of a spinel structure, which possesses high thermal stability, effective dispersion of active mixed metallic particles on the catalyst, increased basic properties, as well as high sintering resistance, which may facilitate a better catalytic performance.

The oxidation of COL over the Mg–Al–Mo HT catalyst was studied by varying the substrate-to-oxidant ratio to 1:1, 1:2, 1:3, and 1:4. The results are presented in Fig. 11. When the substrate-to-oxidant ratio is 1:1, 74% conversion of COL was observed with 30% CAL and 70% epoxy cinnamyl alcohol. Further increase in the substrate-to-oxidant ratio increases the conversion of the reaction. When the substrate-to-oxidant ratio is 1:3, 90% conversion of COL with 33 and 67% selectivity of CAL and epoxy cinnamyl alcohol was observed. Further increase in the ratio (1:4) did not improve the COL conversion significantly.

To understand the reaction rate and calculate the activation energy, the kinetic studies were performed at different temperatures (90, 100, and 110 °C) at different time intervals (30, 60, 90, 120, and 240 min). Linearity of the curve obtained from the ln[*A*] vs. *t* (time) plot implies that the

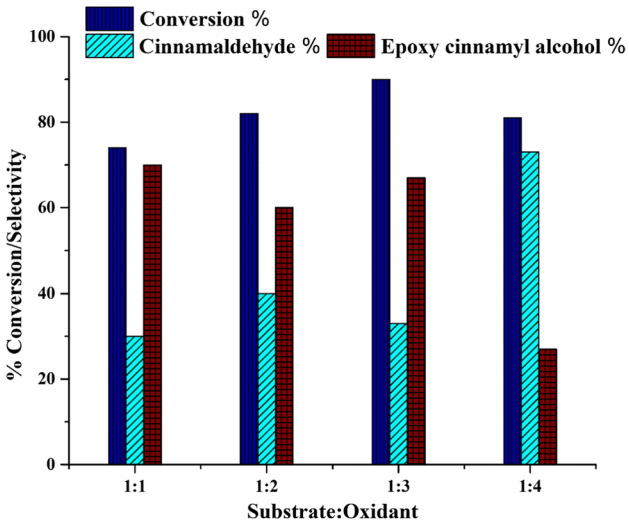

Fig. 11 Effect of substrate-to-oxidant ratio on cinnamyl alcohol oxidation using Mg–Al–Mo HT. #Reaction conditions: 2 mmol COL, 1 mL toluene, 0.05 g catalyst, 110 °C, and 6 h

reaction followed first-order kinetics with respect to cinnamyl alcohol; subsequently, the rate constants were calculated. The Arrhenius plots (ln *K* vs. 1/*T*) obtained for COL oxidation are depicted in the inset of Fig. 12. The slope was calculated to find the activation energy. The data reveal that COL oxidation occurred more rapidly as the temperature increased. The apparent activation energy calculated from the Arrhenius plot was 38.4 kJ.mol^{-1}, which is similar to the literature reports [31].

Based on our study, a possible mechanism for the conversion of cinnamyl alcohol is presented in Scheme 1. During the initial

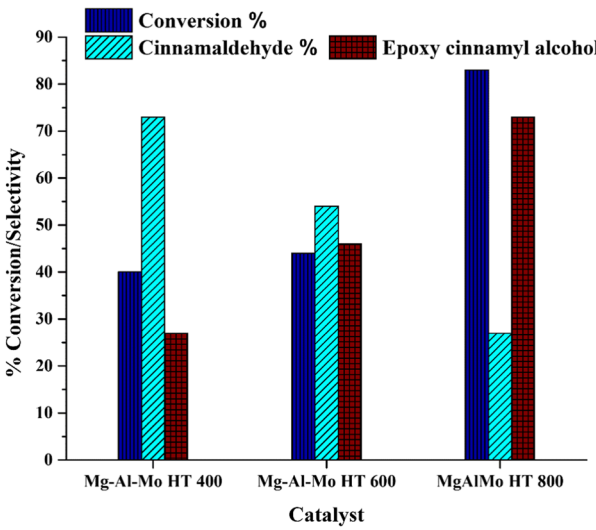

Fig. 10 Effect of calcination temperature of the catalyst on cinnamyl alcohol oxidation. #Reaction conditions: 2 mmol COL, 2 mmol oxidant, 1 mL toluene, 0.05 g catalyst, 110 °C, and 6 h

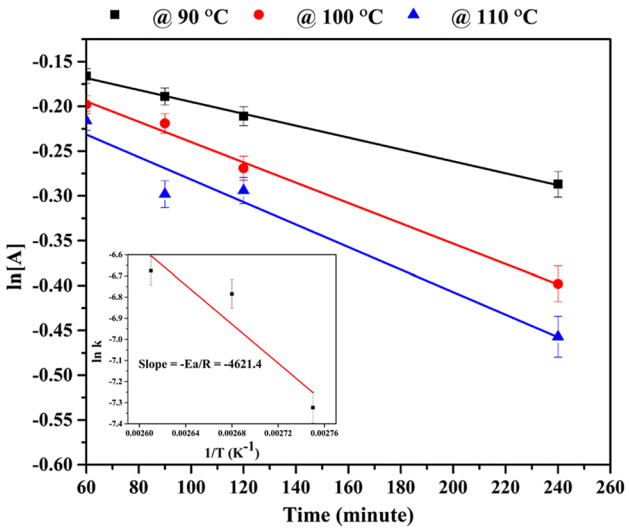

Fig. 12 Kinetic studies on cinnamyl alcohol oxidation reaction over Mg–Al–Mo HT. #Reaction conditions: 2 mmol COL, 2 mmol oxidant, 1 mL toluene, and 0.0 5 g catalyst

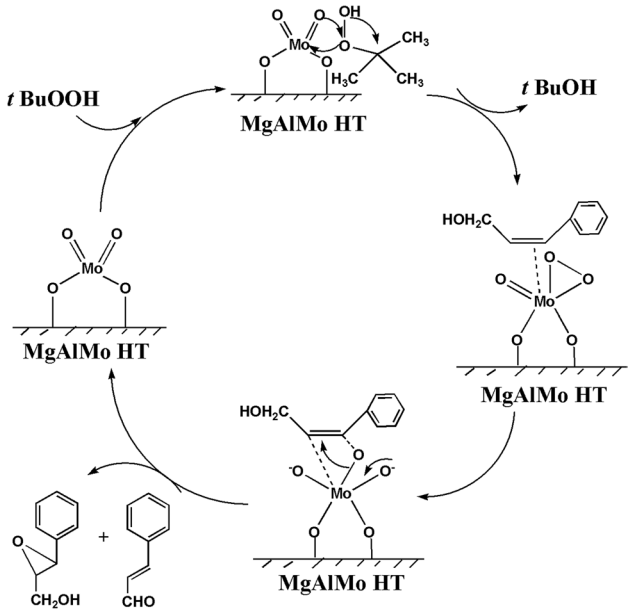

Scheme 1 Possible mechanism of cinnamyl alcohol oxidation in presence of Mg–Al-Mo HT

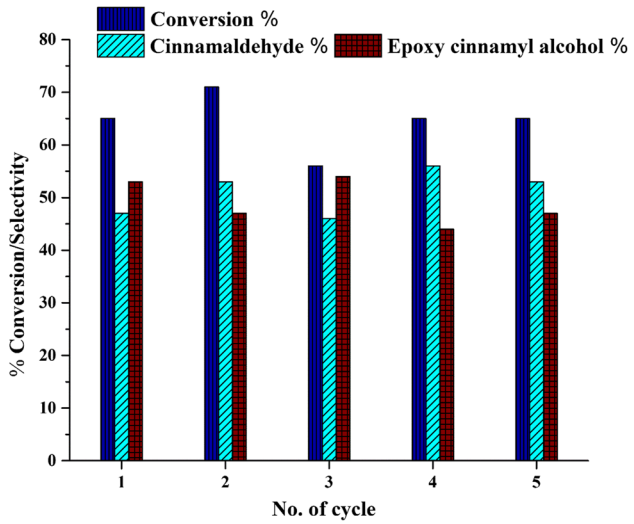

Fig. 13 Recyclability study on Mg–Al–Mo HT catalyst of the cinnamyl alcohol oxidation. #Reaction conditions: 2 mmol COL, 2 mmol oxidant, 0.05 g catalyst, 110 °C, and 6 h

step, chemisorption of peroxide occurs on active molybdenum dioxo-species and forms peroxo-species [35, 36]. The cinnamyl alcohol subsequently chemisorbed on the molybdate sites, dissociated molybdenum peroxo species, and provided the desired epoxycinnamyl alcohol as the product along with cinnamaldehyde. The heterogeneity of the Mg–Al–Mo HT catalyst was followed by the recycling experiments. The recycling experiment was performed by separating the catalyst from the reaction mixture by filtration, followed by washing in isopropanol and drying in an air oven. The results of the recycling experiment are summarized in Fig. 13. The catalyst was active for up to five consecutive reaction cycles without much loss in conversion. The selectivity of CAL and epoxy cinnamyl alcohol remains at ~ 50% in all the cycles.

4 Conclusion

Mg–Al–Mo HT-like material was prepared using the co-precipitation followed by hydrothermal treatment. The formation of the material with hydrotalcite structure was confirmed by FT-IR and powder XRD analysis. The BET surface area analysis confirms the non-porous nature of the sample. The strong acidic sites of the catalyst were identified from the high-temperature desorption peaks obtained by NH_3-TPD analysis. The developed catalyst was explored for the oxidation of COL in both as-prepared and calcined forms. The catalyst obtained by 800 °C calcination showed better activity in the oxidation of COL with 82% conversion and with 27% and 73% selectivity to CAL and epoxy cinnamyl alcohol, respectively. The use of solvents increased the conversion rate of the reaction, and among the various solvents studied, toluene gave better conversion of the reaction. Among the various oxidants, TBHP in decane facilitates the reaction with better conversion and selectivity. The presence of molybdate species in the interlayer region of the HT facilitates the epoxy cinnamyl alcohol. The activity of the catalyst was retained for five consecutive reaction cycles.

Supplementary Information The online version contains supplementary material available at https://doi.org/10.1007/s42247-023-00463-6.

Author contribution M. Dipti Ranjan, A. Sreenavya, and P. P. Neethu: All these authors equally contributed on synthesis and reaction methodology, preparation of materials, characterization and formal analysis, and writing (review and editing). Dr. N. J. Venkatesha: analyzing textural properties and data analysis. Prof. (Dr.) A. Sakthivel: conceptualization, formal analysis, writing (review and editing), funding acquisition, and supervision.

Funding A. Sakthivel is grateful to the DST-SERB-CRG (Project No: CRG/2019/004624) for financial support.

Declarations

Competing interest The authors declare no competing interests.

References

1. V. Rives, Mater. Chem. Phys. **75**, 19–25 (2002). https://doi.org/10.1016/S0254-0584(02)00024-X
2. H. Wang, Z. Yang, X. Zhan, Y. Wu, M. Li, Fuel process. Technol **160**, 178–184 (2017). https://doi.org/10.1016/j.fuproc.2017.02.032
3. F. Cavani, F. Trifiro, A. Vaccari, Catal Today. **11**, 173–301 (1991). https://doi.org/10.1016/0920-5861(91)80068-K

4. T. Baskaran, J. Christopher, A. Sakthivel, RSC. Adv. **5**, 98853–98875 (2015). https://doi.org/10.1039/C5RA19909C
5. Y. Du, Q. Wang, X. Liang, Y. He, J. Feng, D. Li, J. Catal. **331**, 154–161 (2015). https://doi.org/10.1016/j.jcat.2015.08.013
6. I. Delidovich, R. Palkovits, J. Catal. **327**, 1–9 (2015). https://doi.org/10.1016/j.jcat.2015.04.012
7. K.K. Rao, M. Gravelle, J.S. Valente, F. Figueras, J. Catal. **173**, 115–121 (1998). https://doi.org/10.1006/jcat.1997.1878
8. H.L. Huynh, Z. Yu, Energy Tech. **8**, 1901475 (2020). https://doi.org/10.1002/ente.201901475
9. T. Kawabata, N. Fujisaki, T. Shishido, K. Nomura, T. Sano, K. Takehira, J. Mol. Catal. A: Chem. **253**, 279–289 (2006). https://doi.org/10.1016/j.molcata.2006.03.077
10. E. Gardner, T.J. Pinnavaia, Appl. Catal. A: Gen. **167**, 65–74 (1998). https://doi.org/10.1016/S0926-860X(97)00299-8
11. C.E. Ciocan, E. Dumitriu, T. Cacciaguerra, F. Fajula, V. Hulea, Catal. Today. **198**, 239–245 (2012). https://doi.org/10.1016/j.cattod.2012.04.071
12. S. Palmer, R. Frost, T. Nguyen, J. Therm. Anal. Calorim. **92**, 879–886 (2008). https://doi.org/10.1007/s10973-007-8642-2
13. L. Deng, Z. Shi, B. Li, L. Yang, L. Luo, X. Yang, Ind. Eng. Chem. Res. **53**, 7746–7757 (2014). https://doi.org/10.1021/ie402917s
14. P.C.H. Mitchell, S.A. Wass, Appl. Catal. A: Gen. **225**, 153–165 (2002). https://doi.org/10.1016/S0926-860X(01)00862-6
15. R.R. Schrock, A.H. Hoveyda, Angew. Chem. Int. Ed. **42**, 4592–4633 (2003). https://doi.org/10.1002/anie.200300576
16. P.P. Neethu, A. Sreenavya, A. Sakthivel, Appl. Catal. A: Gen. **623**, 118292 (2021). https://doi.org/10.1016/j.apcata.2021.118292
17. V. Chihaia, K. Sohlberg, R. Zăvoianu, A. Cruceanu, O.D. Pavel, E. Angelescu, A.P. Dias, R. Bîrjega, Reac. Kinet. Mech. Catal. **105**, 145–162 (2012). https://doi.org/10.1007/s11144-011-0398-9
18. N.T. Thao, N.D. Trung, D. Van Long, Catal. Lett. **146**, 918–928 (2016). https://doi.org/10.1007/s10562-016-1710-0
19. S. Chhetri, P. Samanta, C.N. Murmu, T. Kuila, J. Composites Sci. **3**, 11 (2019). https://doi.org/10.3390/jcs3010011
20. A.E. Stamate, O.D. Pavel, R. Zavoianu, I. C. Marcu. **10**, 57 (2020). https://doi.org/10.3390/catal10010057
21. T. Mallat, Z. Bodnar, P. Hug, A. Baiker, J. Catal. **153**, 131–143 (1995). https://doi.org/10.1006/jcat.1995.1115
22. I.B. Niklasson, T. Delaine, M.N. Islam, R. Karlsson, K. Luthman, A.T. Karlberg, Contact Derm. **68**, 129–138 (2013). https://doi.org/10.1111/cod.12009
23. Z. Iqbal, M.S. Khan, R. Khattak, T. Iqbal, I. Zekker, M. Zahoor, H.F. Hetta, E.-S. Batiha, E.M. Alshammari, Catalysts **11**, 863 (2021). https://doi.org/10.3390/catal11070863
24. C. Keresszegi, T. Bürgi, T. Mallat, A. Baiker, J. Catal. **211**, 244–251 (2002). https://doi.org/10.1006/jcat.2002.3723
25. A. Abad, C. Almela, A. Corma, H. García, Chem. Commun. **30**, 3178–3180 (2006). https://doi.org/10.1039/B606257A
26. E. Rucinska, P.J. Miedziak, S. Pattisson, G.L. Brett, S. Iqbal, D.J. Morgan, M. Sankar, G.J. Hutchings, Catal. Sci. Technol. **8**, 2987–2997 (2018). https://doi.org/10.1039/C8CY00155C
27. G. Dhinagaran, S. Prashannasuvaitha, M. Muthukumaran, K. Venkatachalam, Catal. Lett. **151**, 1361–1375 (2021). https://doi.org/10.1007/s10562-020-03383-w
28. P.P. Neethu, P. Aswin, A. Sreenavya, S. Nimisha, P.S. Aswathi, A. Sakthivel, Reac. Kinet. Mech. Catal. **135**, 1587–1606 (2022). https://doi.org/10.1007/s11144-022-02211-z
29. R. Dimitrova, Y. Neinska, M.R. Mihályi, T. Tsoncheva, M. Spassova, React. Kinet. Catal. Lett **74**, 353–362 (2001). https://doi.org/10.1023/A:1017909832605
30. M. Salimi, A. Zamanpour, Inorg. Chem. Commun. **119**, 108081 (2020). https://doi.org/10.1016/j.inoche.2020.108081
31. D. Waffel, B. Alkan, Q. Fu, Y. T. Chen, S. Schmidt, C. Schulz, H. Wiggers, M. Muhler, B. Peng, Chem. Plus Chem. 1155–1163 (2019) https://doi.org/10.1002/cplu.201900429.
32. T. Baskaran, R. Kumaravel, J. Christopher, A. Sakthivel, RSC Adv. **4**, 11188–11196 (2014). https://doi.org/10.1039/C3RA46703A
33. S. Kannan, Catal. Surv Asia **103**, 117–137 (2006). https://doi.org/10.1007/s10563-006-9012-y
34. Y. He, J. Feng, G.L. Brett, Y. Liu, P.J. Miedziak, J.K. Edwards, D.W. Knight, D. Li, G.J. Hutchings, Chem. Sus Chem. **8**, 3314–3322 (2015). https://doi.org/10.1002/cssc.201500503
35. A. Sakthivel, J. Zhao, M. Hanzlik, F.E. Kuhn, Dalton Trans. **20**, 3338–3341 (2004). https://doi.org/10.1039/B410634B
36. A. Sakthivel, M. Abrantes, A.S.T. Chiang, F.E. Kuhn, J. Orgnometallic Chem. **691**, 1007–1011 (2006). https://doi.org/10.1016/j.jorganchem.2005.10.054
37. A. Sreenavya, V. Ganesh, N. J. Venkatesha, and A. Sakthivel, Biomass Conv. Bioref. 1–16 (2022) https://doi.org/10.1007/s13399-022-02641-8.
38. Q. Xu, G. Jia, J. Zhang, Z. Feng, C. Li, J. Phys. Chem. C. **112**, 9387–9393 (2008). https://doi.org/10.1021/jp800359p
39. H. Tian, I.E. Wachs, L.E. Briand, J. Phys. Chem. B. **109**, 23491–23499 (2005). https://doi.org/10.1021/jp053879j
40. J. Das, D. Das, K.M. Parida, J. Colloid Inter. Sci. **301**, 569–574 (2006). https://doi.org/10.1016/j.jcis.2006.05.014